Inorganic Chemistry
Article

Inorg. Chem. **2010**, *49*, 905–915 **905**
DOI: 10.1021/ic901621x

Synthesis, Crystal Structures, and Luminescent Properties of Two Series' of New Lanthanide (III) Amino-Carboxylate-Phosphonates

Tian-Hua Zhou, Fei-Yan Yi, Pei-Xin Li, and Jiang-Gao Mao*

State Key Laboratory of Structural Chemistry, Fujian Institute of Research on the Structure of Matter, the Chinese Academy of Sciences, Fuzhou 350002, P. R. China

Received August 13, 2009

Hydrothermal reactions of lanthanide(III) chlorides with 4-HOOC−C_6H_4−$CH_2NHCH_2PO_3H_2$ (H_3L) at different ligand-to-metal (L/M) ratios afforded nine new lanthanide(III) carboxylate-phosphonates with two types of 3D network structures, namely, $LnCl(HL)(H_2O)_2$ (Ln = Sm, **1**; Eu, **2**; Gd, **3**; Tb, **4**; Dy, **5**; Er, **6**) and $[Ln_2(HL)(H_2L)(L)(H_2O)_2]\cdot 4H_2O$ (Ln = Nd, **7**; Sm, **8**; Eu, **9**). Compounds **1**−**6** are isostructural and feature a 3D network in which the LnO_7Cl polyhedra are interconnected by bridging CPO_3 tetrahedra into 2D inorganic layers parallel to the bc plane. These layers are further cross-linked by organic groups of the carboxylate-phosphonate liagnds via the coordination of the carboxylate groups into a pillared-layered architecture. Compounds **7**−**9** are also isostructural and feature a 3D open-framework composed of 1D lanthanide(III) phosphonate inorganic slabs which are further bridged by organic groups of the carboxylate-phosphonate liagnds via the coordination of the carboxylate groups, forming large 1D tunnels along the *b*-axis which are filled by lattice water molecules. Luminescent measurements indicate that compounds **2**, **4**, and **5** show strong emission bands in red, green, and yellow light region, respectively. Magnetic properties of **2**, **3**, **5**, and **7** have also been studied.

Introduction

The search for novel porous inorganic−organic hybrid materials based on metal phosphonates has attracted increasing attention over the past years, mainly owing to their compositional and structural diversities, as well as potential applications in catalysis, ion exchange, magnetism, and materials chemistry.[1−5] These materials with intriguing diversity of architectures, derived from the molecular-scale composite of inorganic−organic components, point the way to design novel electro-optical and sensing materials.[2a,b,6] So far, a great number of metal phosphonates with open-framework structures have been successfully constructed by the careful selection of metal ions and phosphonic acids.[2−6]

Lanthanide phosphonates normally have low solubility in water and organic solvents, hence it is generally difficult to obtain single crystals suitable for X-ray structural analysis.[7−9] Nevertheless the elucidation of the structures of lanthanide phosphonates is very important since these compounds may exhibit useful luminescent properties in both the visible and near IR regions.[7a] To improve the solubility and crystallinity

*To whom correspondence should be addressed. E-mail: mjg@fjirsm.ac.cn.

(1) (a) Clearfield, A. Metal phosphonate chemistry. In *Progress in Inorganic Chemistry*; John Wiley & Sons Inc: New York, 1998; Vol. *47*, pp 371−510.(b) Clearfield, A. *Curr. Opin. Solid State Mater. Sci.* **1996**, *1*, 268–278.

(2) (a) Clearfield, A. *Dalton Trans.s* **2008**, 6089–6102. (b) Férey, G. *Chem. Soc. Rev.* **2008**, *37*, 191–214. (c) Shimizu, G. K. H.; Vaidhyanathan, R.; Taylor, J. M. *Chem. Soc. Rev.* **2009**, *38*, 1430–1449.

(3) (a) Miller, S. R.; Pearce, G. M.; Wright, P. A.; Bonino, F.; Chavan, S.; Bordiga, S.; Margiolaki, I.; Guillou, N.; Férey, G.; Bourrelly, S.; Llewellyn, P. L. *J. Am. Chem. Soc.* **2008**, *130*, 15967–15981. (b) Maeda, K. *Microporous Mesoporous Mater.* **2004**, *73*, 47–55. (c) Fanucci, G. E.; Krzystek, J.; Meisel, M. W.; Brunel, L. C.; Talham, D. R. *J. Am. Chem. Soc.* **1998**, *120*, 5469–5479.

(4) Wu, J.; Hou, H.; Han, H.; Fan, Y. *Inorg. Chem.* **2007**, *46*, 7960–7970.

(5) Chen, Z.; Zhou, Y.; Weng, L.; Yuan, C.; Zhao, D. *Chem. Asian J.* **2007**, *2*, 1549–1554.

(6) (a) Cheetham, A. K.; Férey, G.; Loiseau, T. *Angew. Chem., Int. Ed.* **1999**, *38*, 3268–3292. (b) Rao, C. N. R.; Natarajan, S.; Vaidhyanathan, R. *Angew. Chem., Int. Ed.* **2004**, *43*, 1466–1496. (c) Aspinall, H. C. *Chem. Rev.* **2002**, *102*, 1807–1850. (d) Bünzli, J.-C. G.; Piguet, C. *Chem. Soc. Rev.* **2005**, *34*, 1048–1077.

(7) (a) Mao, J.-G. *Coord. Chem. Rev.* **2007**, *251*, 1493–1520. (b) Ying, S.-M.; Mao, J.-G. *Cryst. Growth Des.* **2006**, *6*, 964–968. (c) Tang, S.-F.; Song, J.-L.; Li, X.-L.; Mao, J.-G. *Cryst. Growth Des.* **2007**, *7*, 360–366. (d) Guo, Y.-Q.; Tang, S.-F.; Yang, B.-P.; Mao, J.-G. *J. Solid State Chem.* **2008**, *181*, 2713–2718. (e) Song, J.-L.; Yi, F.-Y.; Mao, J.-G. *Cryst. Growth Des.* **2009**, *9*, 3273–3277.

(8) (a) Bao, S.-S.; Ma, L.-F.; Wang, Y.; Fang, L.; Zhu, C.-J.; Li, Y.-Z.; Zheng, L.-M. *Chem.—Eur. J.* **2007**, *13*, 2333–2343. (b) Liu, F.-Y.; Roces, L.; Ferreira, R. A. S.; Garcia-Granda, S.; Garcia, J. R.; Carlos, L. D.; Rocha, J. *J. Mater. Chem.* **2007**, *17*, 3696–3701. (c) Ma, Y.-S.; Li, H.; Wang, J.-J.; Bao, S.-S.; Cao, R.; Li, Y.-Z.; Ma, J.; Zheng, L.-M. *Chem.—Eur. J.* **2007**, *13*, 4759–4769. (d) Liu, X.-G.; Zhou, K.; Dong, J.; Zhu, C.-J.; Bao, S.-S.; Zheng, L.-M. *Inorg. Chem.* **2009**, *48*, 1901–1905. (e) Cao, D.-K.; Hou, S.-Z.; Li, Y.-Z.; Zheng, L.-M. *Cryst. Growth Des.* **2009**. ASAP.

(9) (a) Evans, O. R.; Ngo, H. L.; Lin, W. *J. Am. Chem. Soc.* **2001**, *123*, 10395–10396. (b) Groves, J. A.; Wright, P. A.; Lightfoot, P. *Inorg. Chem.* **2005**, *44*, 1736–1739. (c) Zhu, Y.-Y.; Sun, Z.-G.; Chen, H.; Zhang, J.; Zhao, Y.; Zhang, N.; Liu, L.; Lu, X.; Wang, W.-N.; Tong, F.; Zhang, L.-C. *Cryst. Growth Des.* **2009**, *9*, 3228–3234. (d) Sonnauer, A.; Nather, C.; Hoppe, H. A.; Senker, J.; Stock, N. *Inorg. Chem.* **2007**, *46*, 9968–9974.

Published on Web 12/30/2009

Scheme 1. Synthesis of H_3L: (i) $P(OEt)_3$/HCHO/$N(Et)_3$/MeOH, reflux, 4 h. (ii) 20 wt % NaOH/MeOH, reflux, 2 h. (iii) 6 M HCl.

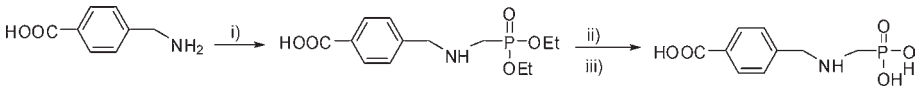

of lanthanide phosphonates, one effective approach is to introduce a variety of additional functional groups such as crown ethers,[10] hydroxy,[8b,11] pyridyl,[7c,8c,12] sulfonate[13], and carboxylates[14,15] to the phosphonate groups. The introduction of a second coligand such as 4,4′-bipy or an oxalate anion has also been demonstrated to be another useful route for the isolation of single crystals of lanthanide phosphonates.[7b,13,14b,14c] In particular, we, as well as others, found that phosphonic acid with an amino-carboxylic acid moiety is a good ligand to design lanthanide(III) phosphonates with novel architectures and luminescent properties.[8e,14a,16] A few chiral lanthanide phosphonates with the amino-carboxylate groups have also been reported that exhibit fascinating structure and strong fluorescent emission in the solid state at room temperature.[17] More recently, lanthanide diphosphonates with 4-HOOC$-C_6H_4-CH_2N(CH_2PO_3H_2)_2$ (H_5L), where the carboxylate group is well separated from the phosphonate part by a rigid benzyl ring, have been also reported.[7e,16d,18] More interestingly, when the oxidizing nitrate anion was present, the in situ oxidation of one P$-$C bond of the H_5L ligand was observed.[16d] Furthermore, by using the squaric acid as the second metal linker, one of the two N$-$C bonds of H_5L was broken under the hydrothermal reactions and a new multifunctional squarato-phosphonate ligand can be formed by the condensation reaction between one C$=$O group of the squaric acid and the amine group of the H_5L, and resultant lanthanide(III) complexes exhibit a novel 3D pillared layered structure.[7e] So far, little is known about lanthanide(III) complexes of 4-[(phosphonomethylamino)methyl]benzoic acid (H_3L = HOOC$-C_6H_4-CH_2$-$NHCH_2PO_3H_2$) which can not be synthesized directly by the Mannich-type reaction of amines with formaldehyde and phosphorous acid.[19] It would be interesting to compare the structures and physical properties of lanthanide(III) complexes of HOOC$-C_6H_4-CH_2NHCH_2PO_3H_2$ with those of corresponding 4-HOOC$-C_6H_4-CH_2N(CH_2PO_3H_2)_2$. Hence we prepared aminomethylenephosphonic acids (H_3L) by using paraformaldehyde, 4-(aminomethyl)benzoic acid, and triethyl phosphite (Scheme 1). Hydrothermal reactions of H_3L with lanthanide (III) chlorides afforded nine novel lanthanide carboxylate-phosphonate hybrids with two types of 3D framework structures, namely, $LnCl(HL)(H_2O)_2$ (Ln = Sm, **1**; Eu, **2**; Gd, **3**; Tb, **4**; Dy, **5**; Er, **6**) and $[Ln_2(HL)(H_2L)(L)(H_2O)_2]\cdot 4H_2O$ (Ln = Nd, **7**; Sm, **8**; Eu, **9**). Herein, we reported their synthesis, crystal structures, and luminescent and magnetic properties.

Experimental Section

Materials and Methods. $LnCl_3$ (Ln = Sm, Gd, Dy, E, and Nd), $LnCl_3\cdot 6H_2O$ (Ln = Eu and Tb), concentrated hydrochloric acid (37%), paraformaldehyde, sodium hydroxide, triethylamine, and methanol were obtained from J&K Chemical Ltd. (China) and used as received. 4-(Aminomethyl)benzoic acid and triethyl phosphite were purchased from Alfa Aesar China (Tianjin) Co. Ltd. The aqueous solutions of NaOH and HCl were prepared in deionized water. Elemental analyses (C, H, N) were performed on a Vario EL III elemental analyzer. Thermogravimetric analyses were carried out on a NETZSCH STA 449C unit at a heating rate of 15 °C/min under a nitrogen atmosphere. IR spectra were recorded on a Magna 750 FT-IR spectrometer photometer as KBr pellets in the 4000$-$400 cm^{-1}. The X-ray powder diffraction data were collected on a Panalytical X'pert Pro MPD diffractometer using graphite-monochromated CuKa radiation in the 2θ range of 5$-$65° with a step size of 0.02°. Photoluminescence analyses were performed on an Edinburgh FLS920 fluorescence spectrometer. The magnetic susceptibility measurements were carried out on polycrystalline samples with a PPMS-9T magnetometer in the temperature range 2$-$300 K and magnetic field up to 8 T. Experimental susceptibilities were corrected for susceptibility of the container and the diamagnetic contributions of the sample using Pascal constants.[20] The ^{1}H NMR spectrum was recorded on a Bruker Avance 400 spectrometer. ESI-MS spectra were recorded on a Finnigan DECAX-30000 LCQ Deca XP ion trap mass spectrometer.

Synthesis of 4-[(Phosphonomethylamino)methyl]benzoic acid (H_3L). The H_3L was synthesized from commercial 4-(aminomethyl)benzoic acid in two steps according to reactions outlined in scheme 1. 4-(Aminomethyl)benzoic acid (5.0 g, 0.032 mol) was dissolved in a mixture of paraformaldehyde (0.98 g, 0.032 mol), anhydrous methanol (200 mL) containing triethylamine (20 mL). The triethyl phosphite (8.8 mL, 0.048 mol) was subsequently added dropwise under rigorous stirring over 1 h. After reacting 4 h, the mixture was cooled. An aqueous solution of 20 wt % sodium hydroxide (24 mL, 0.12 mol) was added and refluxed for 2 h. Methanol and triethylamine were removed by distillation at reduced pressure on a rotary evaporator at about 50 °C. The residual solution was acidified with 6 M hydrochloric acid solution until the pH value reached 1.0. The resulting precipitate of 4-({[ethoxyl(hydroxyl)phosphoryl]methylamino}-methyl)benzoic acid (H_2L = HOOC$-C_6H_4-CH_2NHCH_2P(O)$-$(OH)OCH_2CH_3$) was filtered off and recrystallized from 50 mL of deionized water, followed by vacuum drying to give H_2L in 64% yield (5.6 g). ^{1}H NMR (D_2O): δ 8.0 (d, J = 8.0 Hz, 2H), 7.5$-$7.46 (m, 2H), 4.34 (d, J = 4.8 Hz, 2H), 3.86 (m, 2H), 3.14 (d, J = 12.8, 2H), 1.16 ppm (t, J = 7.08 Hz, 3H). ^{31}P NMR: 10.70 ppm. IR

(10) (a) Vojtisek, P.; Cigler, P.; Kotek, J.; Rudovsky, J.; Hermann, P.; Lukes, I. *Inorg. Chem.* **2005**, *44*, 5591–5599. (b) Plutnar, J.; Rohovec, J.; Kotek, J.; Zak, Z.; Lukes, I. *Inorg. Chim. Acta* **2002**, *335*, 27–35. (c) Ngo, H. L.; Lin, W. *J. Am. Chem. Soc.* **2002**, *124*, 14298–14299. (d) Clearfield, A.; Sharma, C. V. K.; Zhang, B. *Chem. Mater.* **2001**, *13*, 3099–3112.

(11) Silvestre, J. P.; Khadraoui, H.; Gillier, H.; El Manouni, D.; Leroux, Y.; Neuman, A.; Prange, T. *Phosphorus, Sulfur Silicon Relat. Elem.* **2001**, *170*, 91–113.

(12) (a) Gan, X.-M.; Binyamin, I.; Rapko, B. M.; Fox, J.; Duesler, E. N.; Paine, R. T. *Inorg. Chem.* **2004**, *43*, 2443–2448. (b) Gan, X.-M.; Rapko, B. M.; Fox, J.; Binyamin, I.; Pailloux, S.; Duesler, E. N.; Paine, R. T. *Inorg. Chem.* **2006**, *45*, 3741–3745.

(13) Du, Z.-Y.; Xu, H.-B.; Mao, J.-G. *Inorg. Chem.* **2006**, *45*, 9780–9788.

(14) (a) Tang, S.-F.; Song, J.-L.; Li, X.-L.; Mao, J.-G. *Cryst. Growth Des.* **2006**, *6*, 2322–2326. (b) Song, J.-L.; Lei, C.; Mao, J.-G. *Inorg. Chem.* **2004**, *43*, 5630–5634. (c) Song, J.-L.; Mao, J.-G. *Chem.—Eur. J.* **2005**, *11*, 1417–1424.

(15) Li, J.-T.; Zheng, L.-M. *Inorg. Chim. Acta* **2009**, *362*, 1739–1742.

(16) (a) Legendziewicz, J.; Gawryszewska, P.; Gałdecka, E.; Gałdecki, Z. *J. Alloys Compd.* **1998**, *275*−*277*, 356–360. (b) Gałdecka, E.; Gałdecki, Z.; Gawryszewska, P.; Legendziewicz, J. *New J. Chem.* **2000**, *24*, 387–391. (c) Serre, C.; Stock, N.; Bein, T.; Férey, G. *Inorg. Chem.* **2004**, *43*, 3159–3163. (d) Tang, S.-F.; Song, J.-L.; Mao, J.-G. *Eur. J. Inorg. Chem.* **2006**, 2011–2019.

(17) Yue, Q.; Yang, J.; Li, G.-H.; Li, G.-D.; Chen, J.-S. *Inorg. Chem.* **2006**, *45*, 4431–4439.

(18) Bauer, S.; Bein, T.; Stock, N. *J. Solid State Chem.* **2006**, *179*, 145–155.

(19) Redmore, D. *J. Org. Chem.* **1978**, *43*, 996–997.

(20) Kahn, O. *Molecular Magnetism*; VCH Publishers, Inc: New York, 1993; pp 3−4.

Table 1. Summary of Crystal Data and Structural Refinements for **1**−**9**[a]

compound	**1**	**2**	**3**	**4**	**5**	**6**	**7**	**8**	**9**
formula	$C_9H_{14}NO_7PClSm$	$C_9H_{14}NO_7PClEu$	$C_9H_{14}NO_7PClGd$	$C_9H_{14}NO_7PClTb$	$C_9H_{14}NO_7PClDy$	$C_9H_{14}NO_7PClEr$	$C_{27}H_{42}N_3O_{21}P_3Nd_2$	$C_{27}H_{42}N_3O_{21}P_3Sm_2$	$C_{27}H_{42}N_3O_{21}P_3Eu_2$
fw	464.98	466.59	471.88	473.56	477.13	481.89	1126.03	1138.25	1141.47
Space group	*Pnma*	*Pnma*	*Pnma*	*Pnma*	*Pnma*	*Pnma*	$P2_1/c$	$P2_1/c$	$P2_1/c$
a (Å)	23.5128(19)	23.496(2)	23.515(12)	23.480(3)	23.463(13)	23.436(17)	20.891(6)	20.910(5)	20.943(7)
b (Å)	6.8407(5)	6.8277(6)	6.828(3)	6.7749(7)	6.750(4)	6.736(5)	7.1310(18)	7.0901(15)	7.077(2)
c (Å)	8.7416(8)	8.7335(8)	8.743(4)	8.6854(9)	8.658(5)	8.643(6)	27.846(8)	27.823(6)	27.809(9)
β (deg)	90	90	90	90	90	90	107.853(4)	107.611(4)	107.309(4)
V (Å^3)	1406.0(2)	1401.1(2)	1403.8(12)	1381.6(3)	1371.2(13)	1364.5(17)	3948.6(19)	3931.4(15)	3935(2)
Z	4	4	4	4	4	4	4	4	4
D_{calcd} (g·cm^{-3})	2.197	2.212	2.233	2.277	2.311	2.346	1.894	1.923	1.927
μ (mm^{-1})	4.508	4.810	5.057	5.457	5.790	6.492	2.807	3.165	3.366
R_1, wR_2 [$I > 2\sigma(I)$][a]	0.0268, 0.0616	0.0285, 0.0580	0.0218, 0.0465	0.0197, 0.0443	0.0213, 0.0468	0.0258, 0.0582	0.0531, 0.1149	0.0437, 0.1042	0.0422, 0.0999
R_1, wR_2 (all data)[a]	0.0282, 0.0625	0.0347, 0.0605	0.0237, 0.0475	0.0207, 0.0450	0.0225, 0.0473	0.0310, 0.0612	0.0678, 0.1236	0.0492, 0.1080	0.0463, 0.1034

[a] $R_1 = \Sigma||F_o| - |F_c||/\Sigma F_o|$, $wR_2 = \{\Sigma w[(F_o)^2 - (F_c)^2]^2/\Sigma w[(F_o)^2]^2\}^{1/2}$.

(KBr, cm^{-1}): 3386 (m), 2993 (m), 2753 (m), 2607 (w), 1698 (s), 1613 (s), 1579 (s), 1514 (m), 1456 (m), 1423 (m), 1393 (w), 1359 (w), 1317 (m), 1274 (m), 1253 (w), 1193 (m), 1178 (s), 1119 (w), 1105 (w), 1063 (m), 1024 (s), 957 (w), 935 (m), 862 (s), 829 (s), 810 (w), 777 (m), 747 (s), 703 (m), 636 (m), 623 (s), 560 (m), 529 (s), 487 (s). Negative ESI/MS *m*/*e* [ions] 272 [HOOC−C_6H_4−CH_2-$NHCH_2P(O)(OCH_2CH_3)O]^-$. The monophosphonate ethyl ester H_2L obtained as above (5.6 g) was further hydrolyzed in 20 mL of hydrochloric acid solution (6 M) for 10 h. The mixture was evaporated in a vacuum until a solid started to precipitate from a colorless solution. After the mixture was cooled to room temperature, the resulting precipitates were filtered, washed with a small amount of cold water, and vacuum-dried to afford H_3L as a white solid in nearly quantitative yield. ^{1}H NMR (400 MHz, D_2O/NaOH) δ ppm 7.72 (d, J = 7.96 Hz, 2H), 7.31 (d, J = 7.60 Hz, 2H), 3.73 (s, 2H), 2.49 (d, J = 12.60 Hz, 2H). ^{31}P NMR: 16.48. IR (KBr, cm^{-1}): 3351 (m), 2986 (m), 2792 (m), 2622 (w), 1706 (s), 1687 (s), 1616 (s), 1580 (m), 1514 (m), 1460 (w), 1422 (m), 1323 (w), 1300 (w), 1279 (s), 1247 (w), 1208 (w), 1162 (s), 1116 (m), 1091 (m), 1035 (w), 1021 (s), 993 (w), 933 (s), 861 (s), 836 (w), 824 (s), 783 (w), 775 (m), 743 (s), 700 (m), 634 (m), 556 (m), 528 (s), 489 (s). The negative ESI/MS *m*/*e* [ions] 244 [HO_2C−C_6H_4−$CH_2NH_2CH_2PO_3H]^-$.

Preparation of $LnCl(HL)(H_2O)_2$ (Ln = Sm, 1; Eu, 2; Gd, 3; Tb, 4; Dy, 5; Er, 6) and $[Ln_2(HL)(H_2L)(L)(H_2O)_2]\cdot 4H_2O$ (Ln = Nd, 7; Sm, 8; Eu, 9). All nine compounds were prepared by hydrothermal reactions by a similar method. For **1**−**6**, a mixture of H_3L (0.087 g, 0.35 mmol) and $LnCl_3\cdot 6H_2O$ (0.35 mmol) in 10 mL of distilled water with the pH value adjusted to 4.0 by the slow addition of 1 M NaOH solution was sealed into autoclave equipped with a Teflon liner (23 mL) and then heated at 150 °C for 4 days. The final pH values of this reaction media are 1.5−2.0. Crystals of **1**−**6** were collected along with small amount of unidentified powder impurities, which were removed using clean with ultrasonic washer for 1−2 min by placing the sample in 200-mesh gauze and immersed in a solvent including water and ethanol. Crystals of **7**−**9** were obtained by under similar hydrothermal conditions with a H_3L/Ln molar ratio of 3:2. The final pH values of the reaction media are close to 1.5. Compounds **1**−**8** were obtained as single phases in a yield of 20% (26.4 mg), 21.5% (28.6 mg), 19.8% (26.6 mg), 24% (32.4 mg), 17.4% (23.6 mg), 21.6% (29.6 mg), 20% (24.3 mg), and 21% (26.1 mg), respectively. Their purities were confirmed by XRD powder diffraction studies, IR spectra, and elemental analyses (see Supporting Information). A lot of efforts were tried to synthesize the single-phase products of compound **9** such as changing the H_3L/Ln ratios, pH values, and the reaction temperatures, but were unsuccessful. The final products turned out to be a mixture of $EuCl(HL)(H_2O)_2$ and $[Eu_2(HL)(H_2L)(L)(H_2O)_2]\cdot 4H_2O$. Only the IR spectrum for compound **9** was recorded (see Supporting Information); its TGA, luminescence, elemental analysis, and XRD powder diffraction studies were not performed due to insufficient sample available.

Single-Crystal Structure Determination. Single crystals of compounds **1**−**6** and **8**−**9** were performed on a Mercury CCD diffractometer, whereas compound **7** was performed on a Saturn70 CCD diffractometer. Both diffractometers were equipped with graphite-monochromated Mo Kα radiation (λ = 0.71073 Å). Intensity data were collected by the narrow-frame method at 293 K. The data sets were corrected for Lorentz and polarization factors as well as for absorption by the multiscan method.[21] All nine structures were solved by direct methods and refined by full-matrix least-squares fitting on F^2 by SHELX-97.[22] All non-hydrogen atoms were refined with anisotropic thermal parameters. All hydrogen atoms were located at geometrically calculated positions and refined with isotropic thermal parameters. Crystallographic data and structural refinements for compounds **1**−**9** are summarized in Table 1. Important bond lengths are listed in Tables 2 and 3. More details on the crystallographic studies as well as atomic displacement parameters are given as Supporting Information.

Results and Discussion

Compounds **1**−**9** were obtained through hydrothermal reactions of H_3L and the corresponding lanthanide(III) chlorides at 150 °C for 4 days. It has been found that the molar ratio of H_3L/Ln has a strong effect on the chemical compositions and structures of lanthanide phosphonates formed. Compounds **1**−**6** were prepared by using a H_3L/Ln molar ratio of 1:1 whereas compounds **7**−**9** were obtained by using a H_3L/Ln molar ratio of 3:2. These compounds represent the first examples of lanthanide(III) phosphonates of H_3L ligand. They display two types of 3D network structures.

Structural Descriptions for 1−**6.** Compounds **1**−**6** are isostructural. Hence, only the structure of **1** will be discussed in detail as a representative. The asymmetric

(21) *CrystalClear, version 1.3.5*; Rigaku Corp: Woodlands, TX, 1999.
(22) Sheldrick, G. M. *SHELXTL, Crystallographic Software Package version 5.1*; Bruker-AXS: Madison, WI, 1998.

Table 2. Selected Bond Lengths (Å) for Compounds **1**–**6**[a]

compound	1	2	3	4	5	6
Ln(1)−O(1)	2.256(3)	2.247(4)	2.238(3)	2.219(3)	2.209(3)	2.184(4)
Ln(1)−O(2)#1	2.263(3)	2.252(3)	2.250(2)	2.2260(19)	2.211(2)	2.202(3)
Ln(1)−O(2)#2	2.263(3)	2.252(3)	2.250(2)	2.2260(19)	2.211(2)	2.202(3)
Ln(1)−O(3)#3	2.546(3)	2.540(3)	2.537(2)	2.5200(2)	2.509(2)	2.491(3)
Ln(1)−O(3)#4	2.546(3)	2.540(3)	2.537(2)	2.5200(19)	2.509(2)	2.491(3)
Ln(1)−O(3)#6	2.546(3)	2.540(3)	2.537(2)	2.5200(19)	2.509(2)	2.491(3)
Ln(1)−O(2)#7	2.263(3)	2.252(3)	2.250(2)	2.2260(19)	2.211(2)	2.202(3)
Ln(1)−O(1W)	2.536(4)	2.528(4)	2.519(3)	2.500(3)	2.488(3)	2.461(5)
Ln(1)−O(2W)	2.551(4)	2.539(4)	2.537(4)	2.509(3)	2.492(4)	2.478(5)
Ln(1)−Cl(1)	2.8590(15)	2.8546(17)	2.8472(18)	2.8356(11)	2.8281(18)	2.810(2)
P(1)−O(1)	1.492(4)	1.496(4)	1.500(3)	1.495(3)	1.490(3)	1.498(4)
P(1)−O(2)#5	1.501(3)	1.503(3)	1.509(2)	1.505(2)	1.506(2)	1.510(3)
P(1)−O(2)	1.501(3)	1.503(3)	1.509(2)	1.505(2)	1.506(2)	1.510(3)

[a] Symmetry code to generate equivalent atoms: #1 $-x+1/2, -y, z-1/2$; #2 $-x+1/2, y+1/2, z-1/2$; #3 $x+1/2, y, -z+5/2$; #4 $x+1/2, -y+1/2, -z+5/2$; #5 $x, -y+1/2, z$; #6 $x-1/2, y, -z+5/2$; #7 $-x+1/2, -y, z+1/2$.

Table 3. Selected Bond Lengths (Å) for Compounds **7**–**9**[a]

compound	7	8	9
Nd(1)−O(3)#1	2.283(5)	2.262(4)	2.250(4)
Nd(1)−O(13)#2	2.401(4)	2.367(4)	2.365(4)
Nd(1)−O(5)	2.408(4)	2.385(4)	2.368(4)
Nd(1)−O(6)	2.428(5)	2.390(4)	2.377(4)
Nd(1)−O(14)#3	2.466(4)	2.437(4)	2.428(4)
Nd(1)−O(1)#4	2.505(5)	2.491(4)	2.470(4)
Nd(1)−O(1W)	2.685(4)	2.651(4)	2.634(4)
Nd(1)−O(2)#4	2.746(5)	2.727(5)	2.745(5)
Nd(2)−O(7)#5	2.291(4)	2.270(4)	2.269(4)
Nd(2)−O(4)#5	2.325(5)	2.296(4)	2.283(4)
Nd(2)−O(15)#6	2.328(4)	2.316(4)	2.306(3)
Nd(2)−O(8)#7	2.389(4)	2.370(4)	2.363(4)
Nd(2)−O(12)	2.544(5)	2.507(4)	2.495(4)
Nd(2)−O(10)	2.593(5)	2.574(4)	2.570(4)
Nd(2)−O(9)	2.643(5)	2.615(4)	2.608(4)
Nd(2)-O(2W)	2.704(6)	2.620(5)	2.556(5)
P(1)−O(4)	1.509(5)	1.506(4)	1.522(4)
P(1)−O(3)	1.510(5)	1.508(4)	1.511(4)
P(1)−O(5)	1.512(4)	1.516(4)	1.510(4)
P(2)−O(7)	1.504(5)	1.505(4)	1.502(4)
P(2)−O(6)	1.510(4)	1.507(4)	1.512(4)
P(2)−O(8)	1.528(4)	1.525(4)	1.525(4)
P(3)−O(13)	1.501(5)	1.512(4)	1.509(4)
P(3)−O(15)	1.511(5)	1.513(4)	1.515(4)
P(3)−O(14)	1.516(5)	1.518(4)	1.521(4)

[a] Symmetry code used to generate equivalent atoms: #1 $-x, y-1/2, -z+1/2$; #2 $-x+1, -y+1, -z+1$; #3 $-x+1, -y, -z+1$; #4 $x, -y+1/2, z+1/2$; #5 $-x+1, -1/2, -z+1/2$; #6 $x, -y+1/2, z$ - 1/2; #7 $-x+1, y+1/2, -z+1/2$.

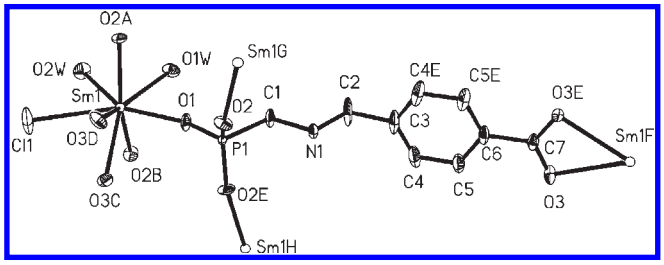

Figure 1. ORTEP drawing of the selected unit in **1** with atomic labeling scheme. Thermal ellipsoids are at the 30% probability level. All H atoms were omitted for clarity. Symmetry codes for the generated atoms: (a) $-x+1/2, -y, z-1/2$; (b) $-x+1/2, y+1/2, -1/2$; (c) $x+1/2, y, -z+5/2$; (d) $x+1/2, -y+1/2, -z+5/2$; (e) $x, -y+1/2, z$; (f) $x-1/2, y, -z+5/2$; (g) $-x+1/2, -y, z+1/2$; (h) $1/2-x, 1/2-y, 1/2+z$.

Scheme 2[a]

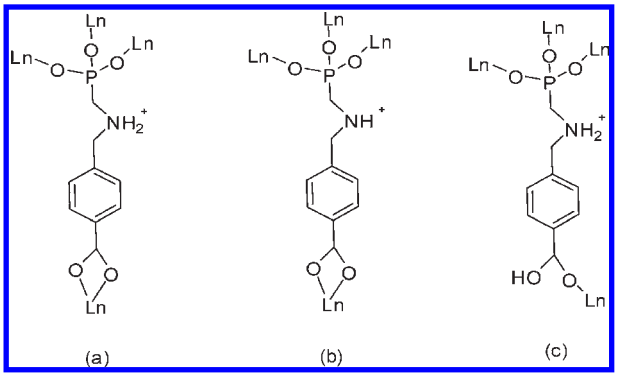

[a] Coordination modes of the phosphonate ligands in compounds **1**–**9**.

unit of **1** consists of one unique Sm (III) ion located at a m site, a HL^{2-} anion passing through a mirror plane, two aqua ligands with a m symmetry, and a chloride anion in a site of mirror plane. As shown in Figure 1, Sm(1) is eight-coordinated by one chloride anion, two aqua ligands, three phosphonate oxygens from three HL^{2-} anions, and a bidentate chelating carboxylate group from another HL^{2-} anion. Its coordination geometry can be viewed as being a distorted bicapped trigonal prism in which Cl and O1W act as two capping atoms. The bond lengths of Sm−O are in the range of 2.256(3) and 2.551(4) Å, which are comparable to those reported for other samarium(III) phosphonates.[7a,16] The Sm−Cl bond length of 2.859(2) Å is much larger than those of Sm−O bonds. The carboxylate-phosphonate ligand is a dianion, the amine group is protonated whereas the phosphonate group and the carboxylate group are deprotonated. The HL^{2-} anion functions as a pentadentate ligand, it chelates with a Sm(III) ion bidentately by using its carboxylate group and also bridges with three other Sm(III) centers by its three phosphonate oxygen atoms. The protonated amino group remains noncoordinated (Scheme 2a).

The Sm^{3+} ions are bridged by tridentate phosphonate groups into a slightly corrugated 2D inorganic layer parallel to the bc plane, forming 6-MR rings (Figure 2a). Both samarium(III) and phosphonate group are 3-connectors in terms of topology, hence the 2D layer can also be described as a three connected sheet with vertex symbol of 6^3. These 2D inorganic layers are cross-linked by organic groups of the phosphonate ligands via the coordination of carboxylate groups (Figure 2b). The benzyl rings of adjacent

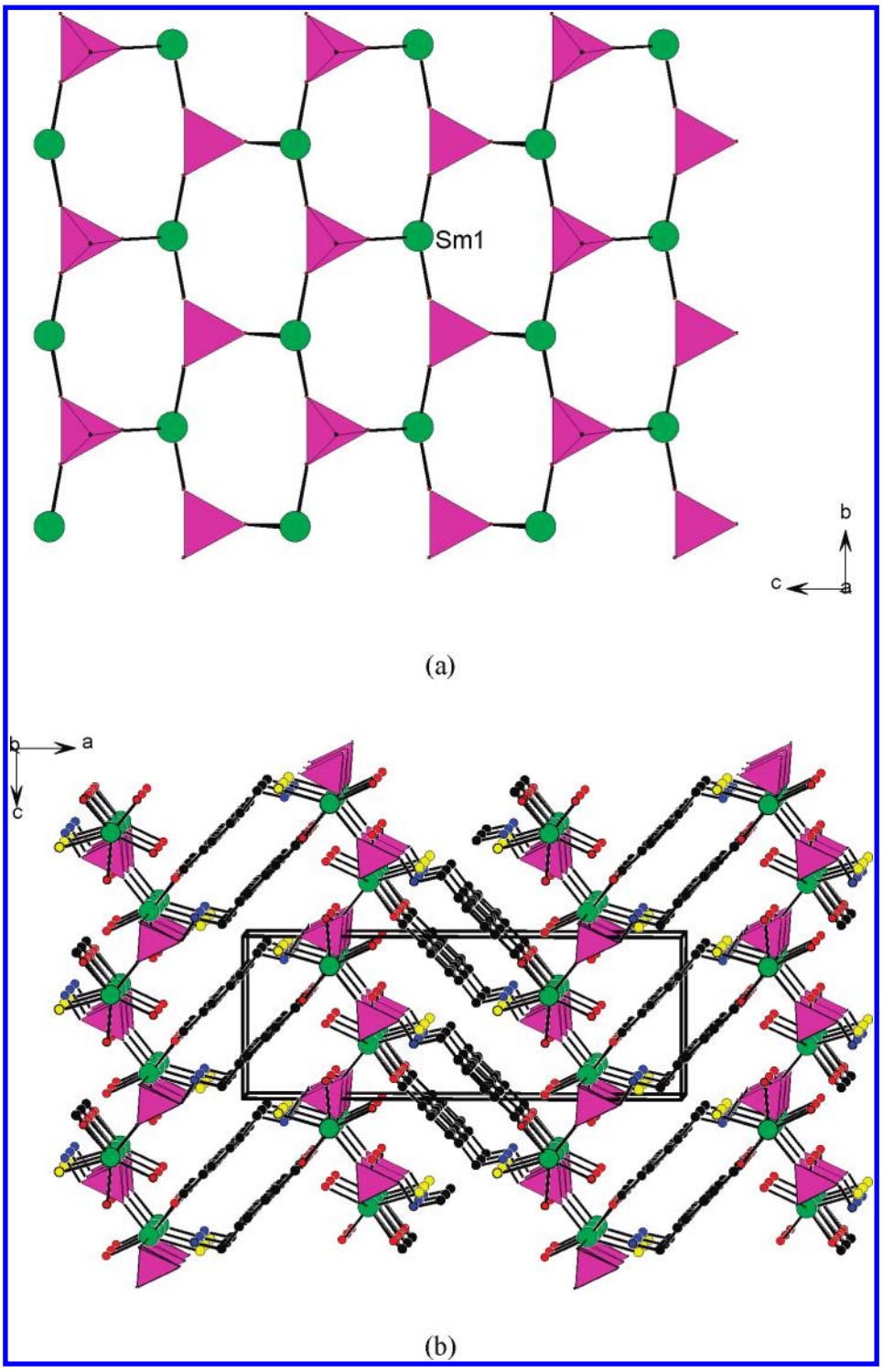

Figure 2. 2D samarium(III) phosphonate inorganic layer in **1** (a) and view of the structure of **1** down the *b* axis (b). CPO_3 tetrahedra are shaded in pink. Sm, Cl, N, C and O atoms are drawn as green, yellow, blue, black, and red circles, respectively.

phosphonate ligands are at least 4.728 Å away from each other, indicating that there is no obvious $\pi-\pi$ stacking interaction. The organic groups of the phosphonate ligands are tilted rather than perpendicular to the inorganic layer, which is due to relatively small interlayer distance of about 10.0 Å. In the lanthanide(III) complexes of 4-HOOC$-C_6H_4-CH_2N(CH_2PO_3H_2)_2$, the lanthanide(III) ions are bridged by the phosphonate groups into 2D or 1D inorganic skeletons which are further interconnected by hydrogen bonds associated with noncoordination carboxylate groups and water molecules into 3D supramolecular architectures. The interlayer distances for those with layered structures are typically larger than 15.0 Å.[16d,18] The erbium(III) complexes of the oxidized ligand, 4-HOOC$-C_6H_4-CH_2N(CHO)-(CH_2PO_3H_2)$ also with a layered inorganic skeleton display a large interlayer space of 21.5 Å since the hydrogen bonds are formed between two $-C_6H_4-$COOH groups aligned linearly.[16d]

It is observed that the Ln−O bond lengths are decreased and the cell volume also contracts about 3.2% from **1** to **6** due to the so-called "lanthanide contraction" (Table 2).

Structural Descriptions of 7−9. Compounds **7−9** are isotructural and feature a different type of 3D framework structure from those of **1−6**. The structure of compound **8** will be discussed in detail as a representative. The asymmetric unit of compound **8** contains two unique Sm(III) ions, three phosphonate ligands carrying 1, 2, and 3 negative charges, respectively, and two aqua ligands as well as four lattice water molecules (Figure 3). Sm1 is eight-coordinated by five phosphonate oxygens and a bidentate chelating carboxylate group from six different carboxylate-phosphonate ligands as well as one aqua ligand. Sm2 is eight-coordinated to four phosphonate oxygens, one bidentate chelating and one monodentate carboxylate groups from six carboxylate-phosphonate ligands and one aqua ligand. The Sm−O distances range from 2.262(4) to 2.727(5) Å, which are comparable to those in **1** and other Sm(III) phosphonates.[7e,14,16]

The three independent carboxylate-phosphonate ligands adopt two different coordination modes (Scheme 2). The ligands containing P(1) and P(2) are pentadentate (Scheme 2a and b), which is similar to that in **1**. However the extent of protonation is different, the one containing P1 atom is fully deprotonated (L^{3-}) whereas the one containing P2 atom is singly protonated on the amine group (HL^{2-}). The phosphonate-carboxylate ligand containing P3 atom is tetradentate. It bridges with three Sm(III) ions via its three phosphonate oxygen atoms and the forth Sm(III) ion via a carboxylate oxygen (Scheme 2c). It is doubly protonated on the amine group and the carboxylate group (O11). The C19−O11 bond length of 1.302(10) Å is significantly longer than that of C19−O12 bond [1.229(9) Å]. This is also reflected from its IR data showing a strong absorption band around 1681 cm^{-1} associated with the COOH.[23]

The Sm(III) ions are bridged by CPO_3 groups into a 1D inorganic ribbon along the *b*-axis (Figure 4a). The width of the ribbon is about 11.0 Å. Neighboring 1D slabs are further cross-linked by the organic groups of the carboxylate-phosphonate ligands into a 3D open-framework with large 1D tunnels along the *b*-axis (Figure 4b). The ligands associated with N1 and N3 atoms join the ribbons in the c-direction whereas those of N2 atoms join along the *a*-axis. The size of the tunnel is estimated to be 6.5 × 6.7 Å based on structural data (the radii of the carbon atoms deducted). The total solvent-accessible space is about 17.6% of the cell volume according to our calculations.[24] The lattice water molecules are located in the above tunnels (Figure 4b). Extensive hydrogen bonds are formed among the phosphonate oxygen atoms, the aqua ligands, and the lattice water molecules, which further stabilize the structure (Figure 4b, Table 4). The N···O distances are 2.865(7) Å for N2···O10 (symmetry code: $-x+1, y+1/2, -z+1/2$), 2.800(7) Å for N2···O9 (symmetry code: $-x+1, y-1/2, -z+1/2$), and 2.742(8) Å for N3···O2 (symmetry code: $-x+1, y-1/2, -z+1/2$). The O···O distances are 2.609(7) Å for O11···O8 (symmetry code: $-x+1, y+1/2, -z+1/2$).

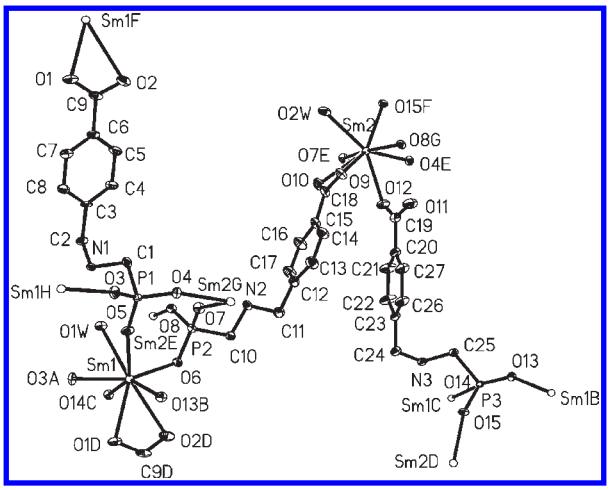

Figure 3. ORTEP drawing of the selected unit in **8** with atomic labeling scheme. Thermal ellipsoids are at the 30% probability level. H atoms and lattice water molecules were omitted for clarity. Symmetry codes for the generated atoms: (a) $-x, y-1/2, -z+1/2$; (b) $-x+1, -y+1, -z+1$; (c) $-x+1, -y, -z+1$; (d) $x, -y+1/2, z+1/2$; (e) $-x+1, y-1/2, -z+1/2$; (f) $x, -y+1/2, z-1/2$; (g) $-x+1, y+1/2, -z+1/2$; (h) $-x, y+1/2, -z+1/2$.

IR and TGA Studies. The IR Spectra of compounds **1−6** are similar, so are those of **7−9**. The broad bands in the range of 3427−3445 cm^{-1} confirm the presence of water molecules in all nine compounds. The absorption bands around 3120 cm^{-1} in **1−6** and 3005 cm^{-1} in **7−9** can be assigned to the aromatic C−H stretching vibrations. The strong bands around 1614 cm^{-1} correspond to the antisymmetric stretching bands of the carboxylate groups, whereas the symmetric stretching bands of the carboxylate group appear at about 1420 cm^{-1}. The bands at around 1681 cm^{-1} in **7−9** can be attributed to the C=O vibration of the carboxylic acid group, suggesting that the COOH group is involved in the formation of hydrogen bonds. The bands from 900 to 1180 cm^{-1} are due to the stretching vibrations of the tetrahedral CPO_3 group.[8b,18,23a,23c,25]

Compounds **1−8** are subjected to TGA studies under a nitrogen atmosphere. TGA curves of compounds **1−6** are similar and exhibit three main steps of weight losses (Figure 5a). Compound **1** was used as an example. It is stable before 160 °C, after which it shows three steps of weight losses. The first step (160−292 °C) corresponds to removal of two aqua ligands. The observed weight loss of 8.4% is slightly higher than the calculated value (7.7%). The second step from 292 to 600 °C corresponds to the removal of the chloride anion and partial combustion of the organic ligand. The third step (600−1000 °C) represents the further decomposing of the compound. The total observed weight loss is 39.1% and the final residuals were not characterized because of the corrosive reactions of the final residuals with the TGA baskets made of Al_2O_3. From the slope of the TGA curve, it is known that the decomposing process is not ended at 1000 °C. TGA curves of **7** and **8** are similar, and each exhibits three

(23) (a) Bauer, S.; Bein, T.; Stock, N. *Inorg. Chem.* **2005**, *44*, 5882–5889. (b) Bellamy, L. J. *Infrared Spectra of Complex Molecules*; Wiley: New York, 1958;(c) Bauer, S.; Marrot, J.; Devic, T.; Férey, G.; Stock, N. *Inorg. Chem.* **2007**, *46*, 9998–10002.

(24) Spek, A. l. *Platon: A Multi-purpose Crystallographic tool*; Utrecht University: Utrecht, The Netherlands, 2001.

(25) Bauer, S.; Muller, H.; Bein, T.; Stock, N. *Inorg. Chem.* **2005**, *44*, 9464–9470.

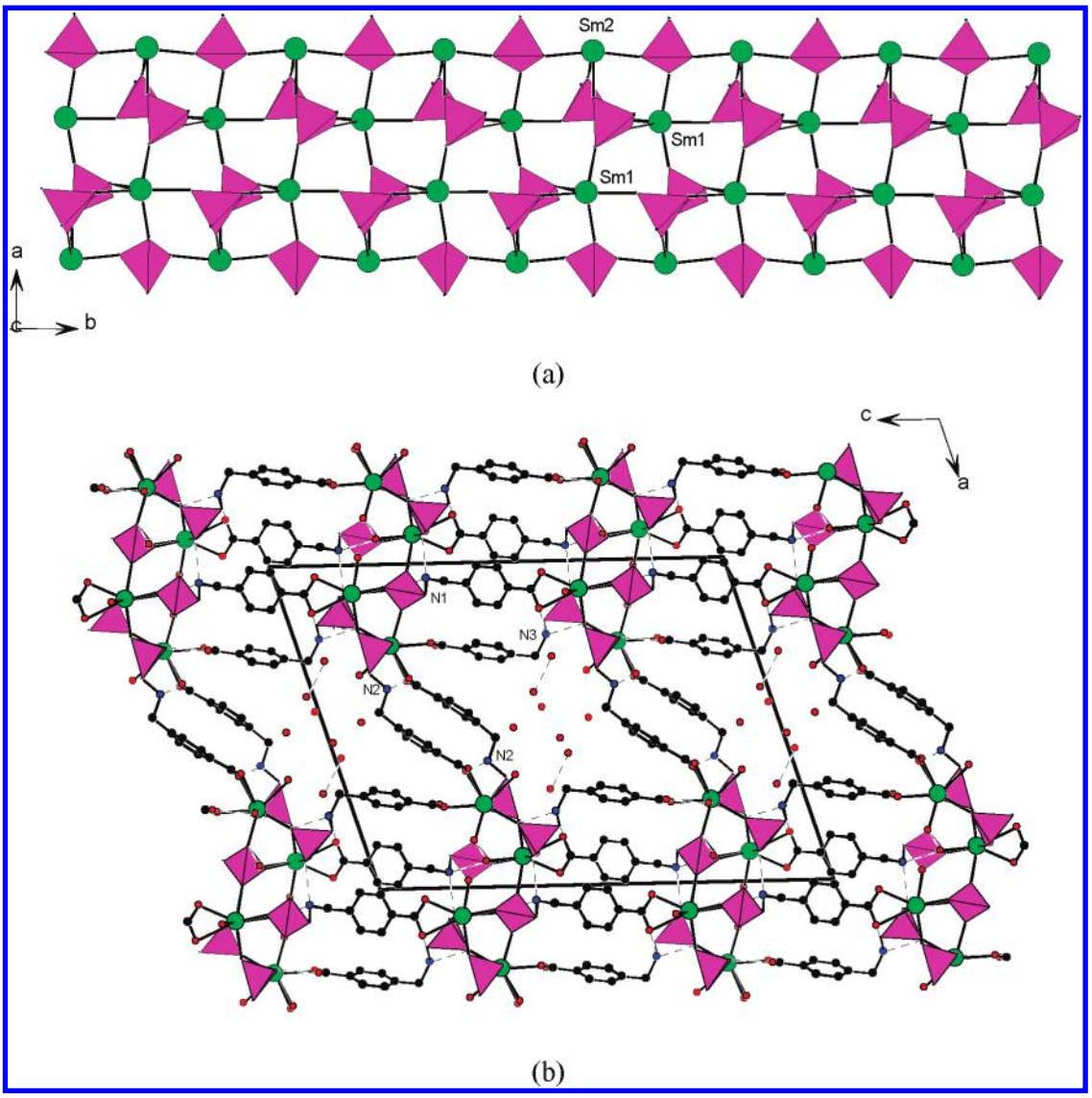

Figure 4. 1D samarium(III) phosphonate inorganic ribbon in **8** (a) and view of the structure of **8** down the *b* axis (b). CPO_3 tetrahedra are shaded in pink. Sm, N, C, and O atoms are drawn as green, blue, black, and red circles, respectively. Hydrogen bonds are drawn as dashed lines.

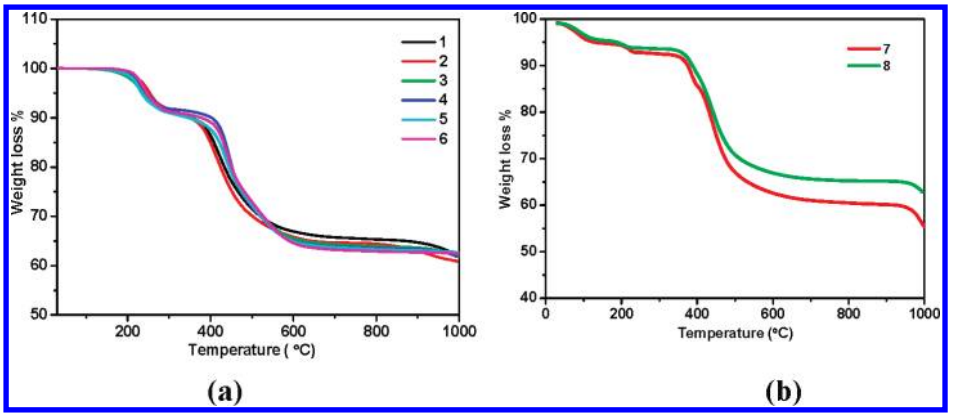

Figure 5. TGA curves for compounds **1**−**6** (a), **7** and **8** (b).

main steps of weight losses, compound **7** is given as an example. The weight loss before 347 °C corresponds to the removal of the four lattice water molecules and two aqua ligands. The observed weight loss of 8.1% is slightly lower than the expected value (9.6%). The second step in the range of 347−602 °C corresponds to the decomposition of the organic ligands. Starting from 950 °C, further weight loss was observed. The total weight losses at 1000 °C are 44.6% and the final residuals were not characterized because of the corrosive reactions of the final residuals

Table 4. Hydrogen Bond Distances (Å) and Angles (°) for **7**−**9**[a]

D−H···A	d(D−H)	d(H···A)	d(D···A)	<(DHA)
compound **7**				
N(2)−H(2C)···O(10)#1	0.90	1.97	2.864(7)	171.6
N(2)−H(2D)···O(9)#2	0.90	1.92	2.801(7)	164.1
N(3)−H(3A)···O(2)#2	0.90	1.87	2.743(8)	161.4
O(11)−H(11C)···O(8)#1	0.82	1.79	2.607(7)	172.0
O(1W)−H(1WC)···O(4)#3	0.85	2.06	2.848(6)	153.0
O(4W)−H(4WB)···O(6W)	0.85	1.92	2.760(18)	171.8
compound **8**				
N(2)−H(2C)···O(10)#1	0.90	1.97	2.860(6)	172.3
N(2)−H(2D)···O(9)#2	0.90	1.92	2.798(6)	163.4
N(3)−H(3B)···O(2)#2	0.90	1.87	2.738(7)	161.4
O(11)−H(11C)···O(8)#1	0.82	1.80	2.616(6)	171.5
O(1W)−H(1WC)···O(4)#3	0.85	2.07	2.846(5)	152.4
O(4W)−H(4WB)···O(6W)	0.85	1.92	2.750(15)	167.3
compound **9**				
N(2)−H(2C)···O(10)#1	0.90	1.96	2.851(6)	172.8
N(2)−H(2D)···O(9)#2	0.90	1.92	2.791(6)	162.5
N(3)−H(3A)···O(2)#2	0.90	1.86	2.734(7)	162.5
O(11)−H(11C)···O(8)#1	0.82	1.80	2.611(6)	172.3
O(1W)−H(1WC)···O(4)#3	0.85	2.07	2.846(5)	152.0
O(4W)−H(4WB)···O(6W)	0.85	1.90	2.728(14)	163.3

[a] Symmetry transformations used to generate equivalent atoms: #1 $-x+1, y+1/2, -z+1/2$; #2 $-x+1, y-1/2, -z+1/2$; #3 $x, y-1, z$.

with the TGA baskets made of Al_2O_3. From the slope of the TGA curve, it is known that the decomposing process is not ended at 1000 °C.

Luminescent Properties. The solid-state luminescent spectra of free amino-carboxylate-phosphonate ligand and **1**−**8** were investigated at room temperature (Figure 6). The free H_3L exhibits a broad fluorescent emission band at 349 nm under excitation at 290 nm (Figure 6a). Compounds **1** and **8** did not display the characteristic emission bands of Sm^{3+} ion, but exhibited a broad ligand-centered fluorescence at 434 nm (λ_{ex} = 335 nm) and 452 nm (λ_{ex} = 390 nm), respectively (Figure 6b and g),[9c] which is greatly red-shifted compared with that of the free ligand. This indicates that the energy absorption of the triplet state of the ligand can not be effectively transferred to the excited state of the Sm^{3+} ion. Compounds **6** and **7** did not show characteristic emission bands of the Er(III) or Nd(III) ion in the near-IR region, which may be ascribed to the "quenching effect" of the aqua ligands and lattice water molecules.[14] Compound **2** exhibits five sets of characteristic emission bands for the Eu(III) ion in the visible region under excitation at 290 nm (Figure 6c). These emission bands are 580 nm (very weak, $^5D_0 \rightarrow {}^7F_0$), 588, 593, and 599 nm (weak, $^5D_0 \rightarrow {}^7F_1$), 614, 618, 621, 625 nm (very strong, $^5D_0 \rightarrow {}^7F_2$), 655 nm ($^5D_0 \rightarrow {}^7F_3$), and 690, 695, 701, 703 nm (very weak, $^5D_0 \rightarrow {}^7F_4$). The splitting of $^5D_0 \rightarrow {}^7F_1$, $^5D_0 \rightarrow {}^7F_2$, and $^5D_0 \rightarrow {}^7F_4$ transition bands is due to the "crystal field effect" of the Eu (III) ion in a C_s symmetry, which led to the complete degeneracy of the $^7F_1$ and the partial degeneracy of the ^{7}Fj (j = 2 and 4) states. The $^5D_0 \rightarrow {}^7F_2$ transition, which is allowed by electric dipole and hypersensitive to environment in the vicinity of Eu (III) ion, is very intense, emitting strong red luminescence. The presence of only one sharp band for the $^5D_0 \rightarrow {}^7F_0$ transition confirms the existence of only one type of Eu(III) cation with a C_s symmetry in the structure. The Eu ($^5D_0$) lifetime ($\lambda_{ex,em}$ = 290, 618 nm) is measured to be 0.36 ms. The emission spectrum of **3** only exhibits a broad blue fluorescent emission band at λ_{max} = 431 nm (λ_{ex} = 322 nm) (Figure 6d), which corresponds to a ligand-centered (LC) fluorescence. The metal-centered (MC) electronic levels of the Gd^{3+} ion are known to be located at 31000 cm^{-1}, which is typically well above the ligand-centered electronic levels of the organic ligands.[7c,14a,14c] Therefore, ligand-to-metal energy transfer and the consequent MC luminescence can not be observed.[7c,14c,26] Compound **4** exhibits four very strong characteristic emission bands for the Tb(III) ion in the visible region under excitation at 378 nm (Figure 6e). These emission bands are 489 nm ($^5D_4 \rightarrow {}^7F_6$), 544 nm ($^5D_4 \rightarrow {}^7F_5$), 591 nm ($^5D_4 \rightarrow {}^7F_4$), and 623 nm ($^5D_4 \rightarrow {}^7F_3$), respectively. Among these emission bands, the strongest one is the green luminescence of $^5D_4 \rightarrow {}^7F_4$ transition. The Tb ($^5D_0$) lifetime of **4** for $\lambda_{ex,em}$ = 378, 489 nm is about 0.54 ms. Compound **5** is yellow-luminescent in the solid state when excited at 348 nm. The two emission bands in compound **5** can be assigned to the $^5D_{9/2} \rightarrow {}^6H_{15/2}$ transition (478 nm) and the $^4D_{9/2} \rightarrow {}^6H_{13/2}$ transition (576 nm) of the Dy^{3+} ion (Figure 6f).[9c]

Magnetic Property Measurements. The temperature-dependent magnetic susceptibility data of compounds **2**, **3**, **5**, and **7** have been measured in the temperature range of 2−300 K. Plots of χM T versus T for the four compounds are shown in Figure 7. Compounds **3** and **7** obeyed the Curie−Weiss law above 25 and 100 K, respectively, whereas compounds **2** and **5** did not obey the law in most of the temperature region. For **2**, its molar susceptibility increases almost linearly from 300 to 110 K, and then it changes very slowly until around 20 K, below which a sharp increase is observed (Figure 7a). The effective magnetic moment (μ_{eff}) at room temperature is measured to be 3.21 μ_B, which is slightly smaller than the expected value of 3.40−3.51 μ_B. Upon cooling, the μ_{eff} decreases continuously because of the depopulation of the levels with nonzero J values.[27] At very low temperature, the μ_{eff} value is close to zero, indicative of a ground state of $^7F_0$ for Eu^{3+} ions.[28] The magnetic susceptibility above 110 K follows the Curie−Weiss law owing to the presence of thermally populated excited states,[28b,29] such magnetic behavior has been reported in other Eu^{3+} coordination polymers.[13,28b,29,30]

For **3**, the room-temperature effective magnetic moments (μ_{eff}) of 7.57 μ_B is slightly smaller than the theoretical values of 7.94 μ_B for an isolated Gd^{3+} ion (S = 7/2) calculated according to the Van Vleck formula.[27] Upon cooling, the μ_{eff} value increases very slowly and reaches 7.86 μ_B at 6 K (Figure 7b), indicating ferromagnetic interaction between magnetic centers. Below 6 K it decreases

(26) Wong, W.-K.; Liang, H.; Guo, J.; Wong, W.-Y.; Lo, W.-K.; Li, K.-F.; Cheah, K.-W.; Zhou, Z.; Wong, W.-T. *Eur. J. Inorg. Chem.* **2004**, *2004*, 829–836.

(27) Van Vleck, J. H. *The Theory of Electric and Magnetic Susceptibilities*; Oxford University: Oxford, U.K, 1932; p 243.

(28) (a) Zhang, Z.-H.; Song, Y.; Okamura, T.-A.; Hasegawa, Y.; Sun, W.-Y.; Ueyama, N. *Inorg. Chem.* **2006**, *45*, 2896–2902. (b) Zhang, Z.-H.; Okamura, T.-A.; Hasegawa, Y.; Kawaguchi, H.; Kong, L.-Y.; Sun, W.-Y.; Ueyama, N. *Inorg. Chem.* **2005**, *44*, 6219–6227.

(29) (a) Wan, Y.; Zhang, L.; Jin, L.; Gao, S.; Lu, S. *Inorg. Chem.* **2003**, *42*, 4985–4994. (b) Zheng, X.; Sun, C.; Lu, S.; Liao, F.; Gao, S.; Jin, L. *Eur. J. Inorg. Chem.* **2004**, 3262–3268.

(30) (a) Yang, J.; Yue, Q.; Li, G.-D.; Cao, J.-J.; Li, G.-H.; Chen, J.-S. *Inorg. Chem.* **2006**, *45*, 2857–2865. (b) Li, P.-X.; Mao, J.-G. *Cryst. Growth Des.* **2008**, *8*, 3385–3389. (c) Li, Y.; Zheng, F.-K.; Liu, X.; Zou, W.-Q.; Guo, Lu, C.-Z.; Huang, J.-S. *Inorg. Chem.* **2006**, *45*, 6308–6316.

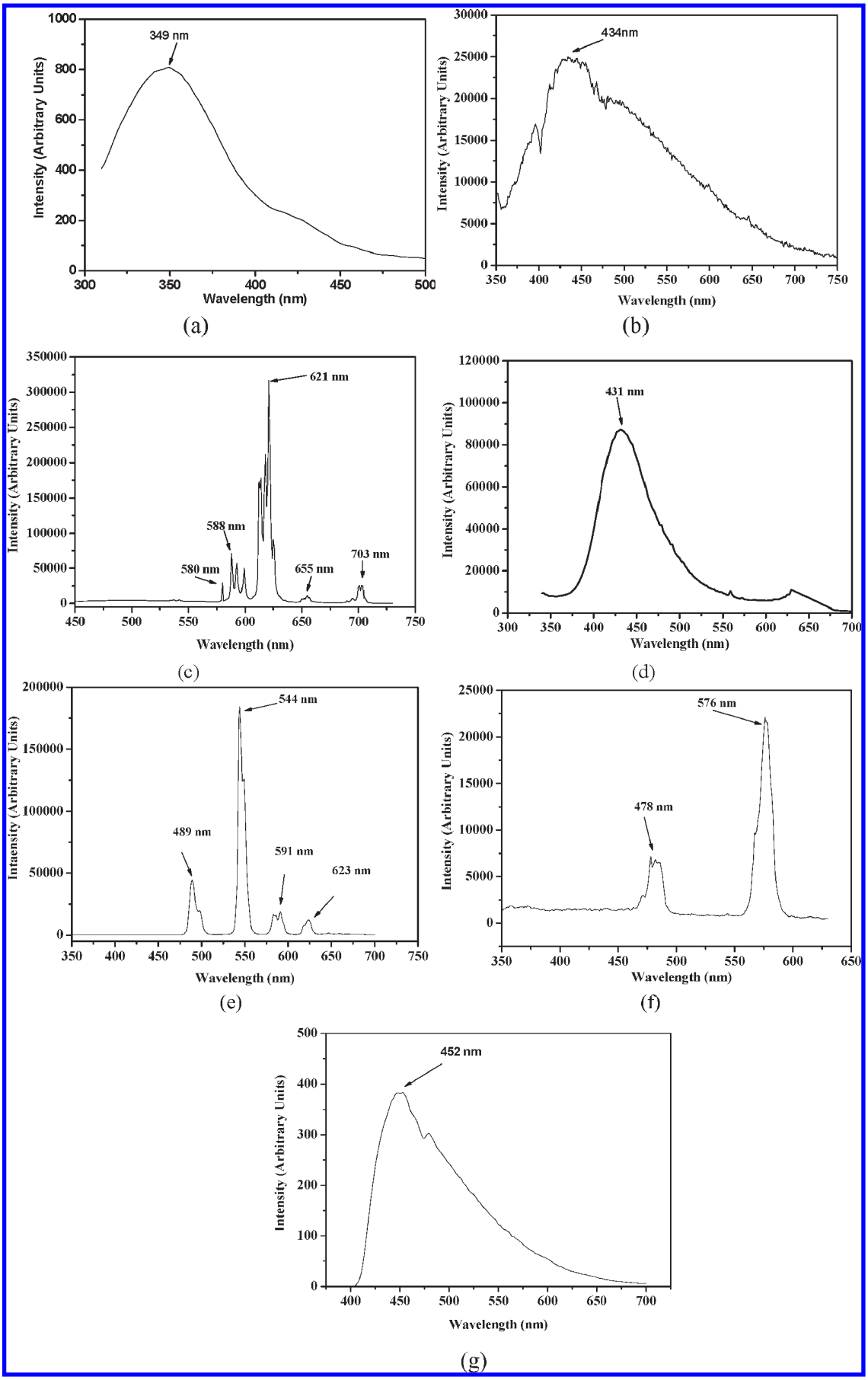

Figure 6. Solid-state emission spectra of H_3L (a), **1** (b), **2** (c), **3** (d), **4** (e), **5** (f), and **8** (g) at room temperature.

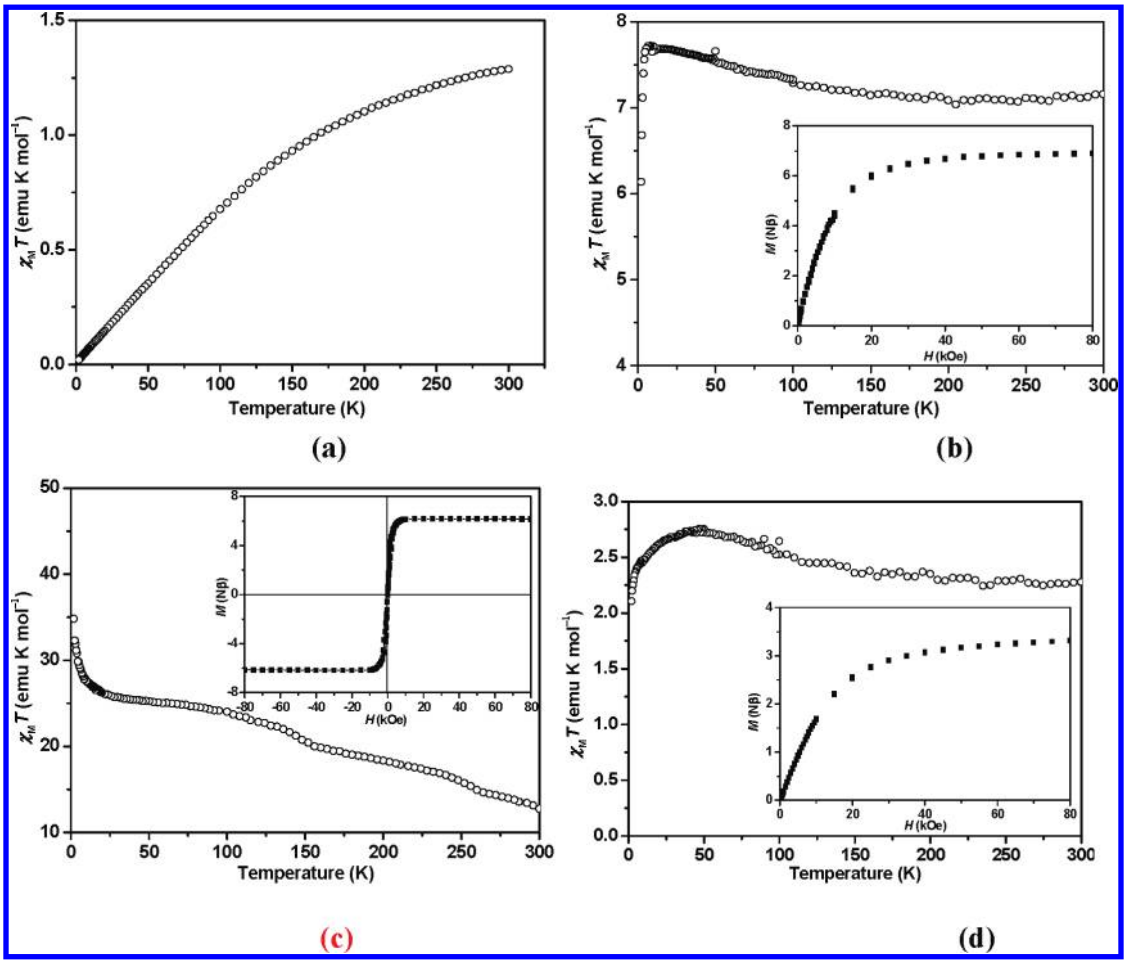

Figure 7. Plots of the temperature dependence of the $\chi_M T$ product for compounds **2** (a), **3** (b), **5** (c) and **7** (d). Inset: magnetization versus field measurement at 2 K on a polycrystalline sample.

more rapidly and reached 7.0 μ_B at 2 K, indicating the presence of possible antiferromagnetic interactions between the layers. Fitting of the data above 25 K according to the Curie−Weiss law gave a Curie constant (C_M) of 7.07 cm^3 K mol^{-1} and a small positive Weiss constant (θ) of 2.06 K. The field dependence of the magnetization of **3** is investigated at 2 K (Figure 7b). The magnetization increases sharply with the increasing magnetic field and saturates at 50 kOe.

For compound **5**, the μ_{eff} value at 300 K is 10.10 μ_B, which is close to the μ_{eff} value expected for an isolated Dy^{3+} ion (10.6 μ_B).[27] As the temperature is lowered, the μ_{eff} value increases steadily and reaches a value of 16.69 μ_B at 2 K. This behavior indicates that the ferromagnetic coupling between Dy^{3+} ions is strong enough to overcome the effect of depopulation of the Stark components of Dy^{3+} due to the splitting of the free-ion ground state, $^6H_{15/2}$, by the crystal field.[28a,30c,31] The ferromagnetic interaction is also confirmed by magnetization measurements in the 0−80 kOe at 2 K (Figure 7c), which increases rapidly with the increasing magnetic field and reaches the saturation value of ca. 6.18 Nβ at 15 kOe. Such type of ferromagnetic behavior has been found in the reported purely three-dimensional Dy^{3+} framework, $\{Dy(TDA)_{1.5}(H_2O)_2\}_n$ [TDA = thiophene-2,5-dicarboxylic acid anion].[31,32,33] It is interesting to note a significant difference between $\{Dy(TDA)_{1.5}(H_2O)_2\}_n$ and compound **5** is the presence of a clear saturation on the M vs H curves of the latter. It is interesting to note that dinuclear or polynuclear dysprosium(III) compounds may also display Singe-Molecule Magnet (SMM) behavior.[34] Currently the origin of different magnetic behaviors in these dysprosium(III) coordination compounds is still not clear.

For **7**, the effective magnetic moment of 4.27 μ_B at room temperature is significantly smaller than the μ_{eff} value for two isolated Nd^{3+} ions (5.20 μ_B) calculated according to the Van Vleck formula.[27] As the temperature is lowered, the μ_{eff} value increases slowly. At 50 K, it reaches a maximum value of 4.69 μ_B and then decreases under further cooling. Fitting of the data above 100 K according to the Curie−Weiss law gave a positive Weiss constant (θ) of 5.7 K and the Curie constant (C_M) of 2.26 cm^3 K mol^{-1}. The field dependence of the magnetization

(31) Chen, Z.; Zhao, B.; Cheng, P.; Zhao, X.-Q.; Shi, W.; Song, Y. *Inorg. Chem.* **2009**, *48*, 3493–3495.

(32) Zhang, X.; Wang, D.; Dou, J.; Yan, S.; Yao, X.; Jiang, J. *Inorg. Chem.* **2006**, *45*, 10629–10635.

(33) (a) Huang, Y.-L.; Huang, M.-Y.; Chan, T.-H.; Chang, B.-C.; Lii, K.-H. *Chem. Mater.* **2007**, *19*, 3232–3237. (b) Andruh, M.; Bakalbassis, E.; Kahn, O.; Trombe, J. C.; Porcher, P. *Inorg. Chem.* **1993**, *32*, 1616–1622.

(34) (a) Hussain, B.; Savard, D.; Burchell, T. J.; Wernsdorfer, W.; Murugesu, M. *Chem. Commun.* **2009**, 1100. (b) Lin, P. H.; Burchell, T. J.; Clerac, R.; Murugesu, M. *Angew. Chem., Int. Ed.* **2008**, *47*, 8848.

of **7** was also investigated at 2 K and showed results similar to those of **3** (Figure 7d).

Conclusions

Nine lanthanide(III) amino-carboxylate-phosphonates with two types of 3D frameworks have been successfully synthesized by using 4-[(phosphonomethylamino)zmethyl]-benzoic acid (H_3L) as a ligand under hydrothermal conditions. Compounds **1**−**6** possess brick-wall-like inorganic layer structures that are further interlinked by the coordination of the carboxylate groups into 3D pillared structures, whereas **7**−**9** feature a 3D framework with large channels along the *b*-axis which are filled by the lattice water molecules. Compounds **2**, **4**, and **5** exhibit strong luminescence in the red, green, and yellow light region, respectively. Results of our studies indicate that the number of phosphonate groups attached to the amino acid has a strong effect on the structures and properties of the lanthanide(III) phosphonates isolated. Our future research efforts will be devoted to the syntheses, crystal structures, and luminescent properties of lanthanide(III) compounds of other related amino-carboxylate-phosphonate ligands.

Acknowledgment. This work was supported by National Natural Science Foundation of China (20973170, 20825104, and 20821061), Key Project of Chinese Academy of Sciences (KJCX2-YW-H01), and 973 Program (2006CB932903), the major project from FJIRSM (SZD09001).

Supporting Information Available: X-ray crystallographic files in CIF format for compounds **1**−**9**; elemental analyses, IR data, simulated and experimental XRD powder patterns for compounds **1**−**8**. This material is available free of charge via the Internet at http://pubs.acs.org.